THE JOURNAL OF PHYSICAL CHEMISTRY B

Article

pubs.acs.org/JPCB

Quantifying Transient 3D Dynamical Phenomena of Single mRNA Particles in Live Yeast Cell Measurements

Christopher P. Calderon,*[,†] Michael A. Thompson,[‡,∥] Jason M. Casolari,[§,⊥] Randy C. Paffenroth,[†] and W. E. Moerner*[,‡]

[†]Numerica Corporation, Loveland, Colorado 80538, United States

[‡]Department of Chemistry, Stanford University, Stanford, California 94305, United States

[§]Department of Biochemistry, Stanford University, Stanford, California 94305, United States

Supporting Information

ABSTRACT: Single-particle tracking (SPT) has been extensively used to obtain information about diffusion and directed motion in a wide range of biological applications. Recently, new methods have appeared for obtaining precise (10s of nm) spatial information in three dimensions (3D) with high temporal resolution (measurements obtained every 4 ms), which promise to more accurately sense the true dynamical behavior in the natural 3D cellular environment. Despite the quantitative 3D tracking information, the range of mathematical methods for extracting information about the underlying system has been limited mostly to mean-squared displacement analysis and other techniques not accounting for complex 3D kinetic interactions. There is a great need for new analysis tools aiming to more fully extract the biological information content from in vivo SPT measurements. High-resolution SPT experimental data has enormous potential to objectively scrutinize various proposed mechanistic schemes arising from theoretical biophysics and cell biology. At the same time, methods for rigorously checking the statistical consistency of both model assumptions and estimated parameters against observed experimental data (i.e., goodness-of-fit tests) have not received great attention. We demonstrate methods enabling (1) estimation of the parameters of 3D stochastic differential equation (SDE) models of the underlying dynamics given only one trajectory; and (2) construction of hypothesis tests checking the consistency of the fitted model with the observed trajectory so that extracted parameters are not overinterpreted (the tools are applicable to linear or nonlinear SDEs calibrated from nonstationary time series data). The approach is demonstrated on high-resolution 3D trajectories of single *ARG3* mRNA particles in yeast cells in order to show the power of the methods in detecting signatures of transient directed transport. The methods presented are generally relevant to a wide variety of 2D and 3D SPT tracking applications.

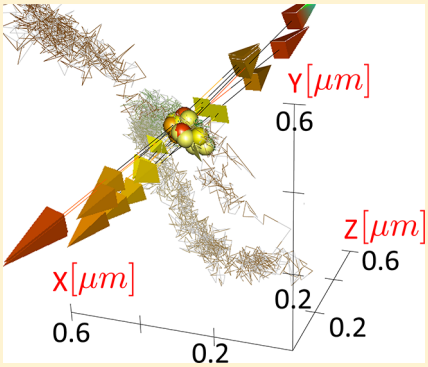

INTRODUCTION

Optical microscopy can now provide high resolution two- (2D) and three-dimensional (3D) measurements of individual biomolecule motion in living cells. The ability to track biomolecules at single-molecule resolution in their native environment permits researchers to address open questions in various fields, e.g.,[1−12]. Time-ordered 3D measurements can assist in providing unambiguous physical interpretations regarding how tagged particles dynamically interact with structures in living cells.[1,3,10,13] Analyzing transient 3D kinetic phenomena in live cell measurements poses new and exciting statistical modeling challenges.

Many early single particle tracking (SPT) analysis methods aimed to quantify single-molecule kinetics by assuming relatively simple stochastic motion models which leveraged either mean square displacement (MSD) methods[14−18] or autocorrelation-based (AC) techniques[19] to extract model parameters summarizing the experimental data. AC methods (time or Fourier domain) often require signals to be stationary; this stationarity assumption can be problematic in several single-molecule situations where the dynamics changes in real time.[20−22] Classic MSD methods lose valuable temporal information due to the aggregation of lag information from different time points and also require researchers to select heuristic tuning parameters.[16]

Improvement in experimental resolution and problems with the aforementioned analysis approaches have motivated new SPT analysis techniques. For example, ref 23 presents a new scheme for systematically selecting the "time-lag" parameter required for extracting both the diffusion coefficient and localization precision (or measurement noise) from an MSD curve. In addition, more statistically motivated methods have been proposed that aim to make better use of time-ordered

Special Issue: Michael D. Fayer Festschrift

Received: June 28, 2013
Revised: September 6, 2013
Published: September 9, 2013

observations. These include maximum likelihood[24] and Bayesian estimation strategies.[25,26] For example, ref 25 demonstrated Bayesian techniques accounting for 2D force interactions in membrane diffusion simulations. These prior efforts, though insightful, did not rigorously account for the statistical effects of *a priori* unknown measurement noise. The measurement noise estimation issue has been discussed recently;[20,27] likelihood-based procedures for extracting parameter estimates treating measurement noise in simple SPT diffusion-only models (e.g., models neglecting 2D/3D force) have been recently introduced.[28]

Moreover, existing SPT analysis methods still encounter three serious technical problems: (i) Methods often require researchers to subjectively specify the types of motion followed by the experimental data. (ii) Many existing methods do not utilize statistically justified methods for checking the consistency of assumed motion models against experimental single-molecule SPT data. (iii) Even if modeling assumptions are consistent, estimation techniques typically assume that the parameters of the motion model are not slowly changing over time in a single trajectory.

With respect to (i), qualitative motion types like "directed", "corralled (or confined)", and "diffusive" are often assumed. SPT researchers typically classify the motion type describing the experimental data and then extract parameter estimates depending on the assumed motion type (various heuristic criteria are used to guide motion classification, e.g., ref 10 and 29). It would be advantageous to consider an estimation scheme that nests all popular SPT models as special cases (i.e., the experimental data "speaks for itself") while also permitting more flexibility in accounting for different types of 2D or 3D forces. Regarding (ii), a parameter estimate and model can be extracted from any data set, but this does not imply that the estimate and model reflect the actual experimental situation. Before one worries about extracting optimal parameter estimates, the consistency of modeling assumptions compared to data should be checked; the value of a parameter estimate predicated on an inapplicable model is not high. This article demonstrates how goodness-of-fit hypothesis testing (i.e., statistical methods for directly determining if an observed time series is consistent with a given model) can assist in analyzing SPT data. Regarding (iii), it is well-known that the local microenvironment and/or properties of the underlying biomolecule can cause the diffusion coefficient to change over time.[16,30,31] A wide variety of anomalous diffusion approaches have been proposed to handle SPT trajectories experiencing changing effective diffusion coefficients, e.g.,[32,33] but such approaches still induce temporal averaging of increments, which can hide important transient single-molecule kinetic phenomena (quantitative examples are provided in the Results and Discussion and the Supporting Information (SI)). Likelihood ratio[24] and Bayes factor-based techniques[34] for identifying abrupt state changes have been proposed for special case situations where the dynamic models fall into one or several discrete states, but these methods assume that one possesses *a priori* reliable statistical information describing the system's stochastic motion and that the states can be discretely classified. In the next section, we discuss other approaches aiming to extract kinetic information from single-molecule trajectories[20,21,25−28,32,34−38] and contrast these approaches to our methods, which offer solutions to items (i)−(iii).

To motivate our work, consider the following example. Suppose one is interested in tracking a complex molecular aggregation process, e.g., ribonucleoprotein complex formation,[39] where the aggregate's radius changes in a nontrivial fashion over the course of an experimental trajectory. If the effective hydrodynamic radius of the aggregate containing one or more fluorescently tagged particles has a "state change" that is effectively continuous (i.e., the radius length changes by small amounts between adjacent frames but the radius changes appreciably over multiple frames), then many existing SPT approaches would encounter serious technical difficulties in both parameter estimation and detecting state changes. Worse yet, the estimated parameters of traditional SPT models would be of questionable quality since the assumptions behind the models are inconsistent with the molecular motion underlying the experimental data.

In order to demonstrate how our proposed approach can provide both estimation and goodness-of-fit hypothesis testing in scenarios where the system dynamics are inconsistent with traditional SPT models and/or parameters are time varying, we analyze 3D *ARG3* mRNA trajectories measured in live *Saccharomyces cerevisiae*.[10] This system was selected because only one or two copies of the mRNA are present in the cytoplasm at any given time,[10,40,41] thus associating a fluorescent signal between different image frames measured by the microscope with a single molecule is straightforward. Simulations and experiments demonstrate what types of 3D dynamical interaction effects can be extracted from individual trajectories. We also discuss how ideas ported from other disciplines[42−47] can help to identify signatures of subtle molecular interactions in biophysical measurements that are not explicitly accounted for in models commonly used in analyzing SPT data.

THEORETICAL METHODS

Qualitative SPT Modeling Background. In single-molecule studies, the emphasis is on avoiding ensemble averaging since each experimental trajectory is associated with different unresolved latent features (e.g., different conformational molecular degrees of freedom or varying local microenvironments). The unresolved latent features often induce substantial "heterogeneity" in the dynamics.[7,10,16,48,49] No pair of trajectories are exactly alike, but researchers in biophysics and cell biology are interested in accurately quantifying/understanding this heterogeneity.[7,10] Therefore, it is important to consider methods that can not only estimate models on a trajectory-wise basis,[36,50] but it is also critical to check the consistency of a estimated model against the single-molecule trajectory used to obtain the parameter estimates.[36,51] Goodness-of-fit testing is crucial since inferring model parameters that have a biophysical interpretation requires researchers to both (1) make testable assumptions about the effective dynamical models and (2) develop schemes for estimating the parameters respecting the complex nature of effective thermal and measurement noise associated with the experimental data. The methods employed in this study permit trajectory-wise goodness-of-tit testing and also check all distributional dependence assumptions[43] implied by an assumed model against observed experimental data directly. The methods utilized are general[43,52] and are not constrained to linear or Gaussian dynamics; advantages of the goodness-of-fit approach are discussed in the Methods, the SI, and elsewhere.[51]

The techniques presented not only handle trajectory-to-trajectory heterogeneity, but can also identify transient

dynamical phenomena occurring in a single trajectory (e.g., an unobserved conformational degree of freedom may be changing in an appreciable fashion over the course of a single trajectory measurement). The trajectory-wise goodness-of-fit testing employed is crucial for identifying these phenomena. Problems other popular methods (e.g., MSD-based analyses) encounter when the dynamical parameters of the system slowly change over time in a single trajectory are discussed and demonstrated using simulation and experimental data in the main text and the SI.

Since checking the consistency of fitted stochastic models against experimental SPT data is of paramount importance to any quantitative scientific SPT study, it may be surprising that such methods are not widely utilized in SPT data analysis. A major reason underlying why the goodness-of-fit testing issue has not been thoroughly studied in SPT works is that the time series coming from these experiments pose technical challenges (e.g., nonstationary signals with potential nonlinear dynamics on top of measurement noise corrupting state observations). Recent research emerging from time series analysis and econometrics are able to address some long-standing technical challenges that previously complicated goodness-of-fit testing associated with complex, transient (i.e., nonstationary) 2D or 3D signals in the past.[43−47] The SI provides simulation examples showing how standard time series diagnostics not checking all distributional assumptions can fail in situations relevant to our SPT study.

Other Related Works. The methods presented here overlap in goals with some other recent efforts aiming to analyze the time series of single-molecule experimental data. In this subsection, we briefly summarize some related efforts. The research closest in spirit to the 3D SPT work presented here can be found in refs 20, 21, and 36, where 1D linear and nonlinear stochastic differential equations (SDEs) are estimated and trajectory-wise goodness-of-fit tests checking all model assumptions[43] are applied to experimental single-molecule trajectories subjected to external force manipulation. Bayesian estimation techniques aiming to achieve efficient parameter estimation in situations where an accurate 2D SDE model is assumed known *a priori* have recently been developed and demonstrated on simulated SPT trajectories.[25] Methods falling under the category of "*p*-variation" methods have been proposed for estimating and testing 1D SPT data in situations where experimental measurement noise is small compared to inherent thermal fluctuations.[32] References 27 and 28 demonstrate various approaches for estimating simple 1D SDE models in the presence of measurement noise; these works also provide discussions outlining the advantages of applying likelihood-based methods to estimate SDE parameters. Reference 26 applied hidden Markov models to characterize complex diffusion patterns in situations where accurate SDE models describing experimental data were assumed known *a priori*; the technique showed promise for quantifying complex protein diffusion patterns in live bacterial cell lines.

In this work, 3D SDE models are estimated from experimental data and measurement noise is inferred using maximum likelihood estimation (MLE). Furthermore, the methods allow one to resolve effectively continuous changes in SDE parameters over time, we employ a flexible modeling framework imposing relatively few *a priori* assumptions about the particle's dynamics (popular SPT models, such as directed and confined diffusion, are covered within a single parametric framework[10,29]), and the consistency of the assumed/fitted model is checked directly against individual experimental trajectories in a trajectory-wise fashion (i.e., goodness-of-fit hypothesis tests checking the consistency of all model assumptions can be carried out using only one experimental trajectory). No other published SPT work provides a framework allowing for all of these features (the 2D/3D goodness-of-fit testing accounting for measurement noise is not provided in any SPT work to our knowledge). Accounting for (and detecting) time-changing parameters characterizing 2D and/or 3D SDE models, e.g., effective measurement noise that is changing significantly over time for a single trajectory, is another contribution of this work (other numerical approaches for quantifying effective continuous parameter changes in single-molecule trajectories are discussed in ref 53).

In terms of other potential SPT modeling approaches, nonlinear filters (such as particle filters[35] and interacting multiple model filters[37]) are tools that show promise when both measurement noise and particle dynamics are accurately known *a priori*, but these nonlinear filtering techniques do not address goodness-of-fit or parameter estimation issues directly. For situations expanding the utility of interacting multiple model filters to scenarios where model parameters and/or priors are not known *a priori*, "non-parametric" Bayesian methods show some promise.[38] However, one still must make some assumptions regarding the statistical nature of the dynamics and measurement noise; furthermore, the approach used in ref 38 does not address the goodness-of-fit question. More broadly, Bayesian methods (like those in refs 25, 26, 34, and 38) by themselves cannot determine whether the assumed dynamical models are statistically consistent with experimental data. For example, it is possible that the Bayesian modeler assumes a collection of models all having Gaussian measurement noise with some fixed variance, but the true data generated by the actual experimental situations is Poisson distributed with a time varying intensity (or worse yet, draws may come from a time-varying unknown distribution); Bayesian model selection[54] approaches would attempt to find the best model in the assumed model class (e.g., parametric models assuming a Gaussian measurement noise process). Once the best model is in hand, uncertainty estimates can be extracted from the computed posterior distribution; this uncertainty depends not only on the "best" model, but also on the real data and the assumed prior distribution, which may also be inconsistent with real experimental data. One can extract a single parameter estimate from the posterior and then apply frequentist goodness-of-fit testing,[51] but the assumed prior may substantially affect the results.

The methods used here aim to detect any inconsistency of the data with modeling assumptions, whereas a pure Bayesian method cannot detect that the observed data exhibits features outside of the class of dynamical models considered.[51] We should explicitly point out two limitations of the goodness-of-fit methods advocated herein: (i) rejection of a fitted model does not specifically point out what is incorrect about the model, and (ii) some modeling assumptions may be incorrect (e.g., the diffusion coefficient is state or position dependent[20]) but there is not enough evidence in the data (i.e., the sample size is too small) to reject the null hypothesis. The power of the testing procedure depends on the true data, the assumed model, and the data sampling frequency.[43] Despite these limitations, the formal goodness-of-fit hypothesis testing machinery shows great promise in quantitatively and more objectively studying experimental single-molecule data.

At a high-level, our method processes individual experimental trajectories by (1) selecting parametric SDE model(s); (2) dividing the trajectory into disjoint time windows; (3) within each window extract the MLE vector summarizing the forces, diffusion, localization precision in that local time window for each model under consideration; (4) checking all of the statistical assumptions implicit in the assumed model against data via goodness-of-fit tests; and (5) if the goodness-fit tests are not rejected and multiple models are under consideration, select a parametric model via model selection criteria (if rejection occurs, consider a new model class and repeating procedure).

General SDE Model Considered. We consider estimation and statistical inference problems associated with an SDE of the form:

$$dr_t = \Phi F(r_t)\, dt + \sqrt{2}\sigma\, dB_t \tag{1}$$

$$\psi_{t_i} = r_{t_i} + \varepsilon_{t_i} \tag{2}$$

where the 3D position of the particle at time t is denoted by the vector $r_t \equiv (x_t,y_t,z_t)^T$ (the superscript denotes a matrix transpose). The subscript t is used to index time in the stochastic process. B_t represents a standard 3D Brownian motion process. The notation dB_t is used as shorthand for an Ito[55] stochastic integral (similarly for dr_t). The remaining terms (and their physical interpretation) in eq 1 will be described in greater detail after additional notation is established. Stochastic effects inherent to SPT experiments, such as photon count uncertainty, prevent us from directly observing r_t. The only quantity we can directly measure in the lab is denoted by ψ. This process is also indexed by time, e.g. ψ_{ti}, but measurements are only available at discrete time points. The random variable ε_{t_i} represents one 3D measurement noise realization at time t_i.

We use the notation $\varepsilon_{t_i} \sim \mathcal{N}(0,R)$ to convey that ε_{t_i} is assumed to be distributed according to a mean zero multivariate Gaussian with covariance R. Using an R inconsistent with the value associated with an experimental trajectory (or assuming an incorrect measurement error distribution) may bias parameter estimates of physically interesting quantities. Motivated by these considerations, we estimate the inferred measurement noise from the observed data using likelihood methods. In SPT applications, R is often unknown *a priori* because the number of photons available for detection decreases during data collection. Furthermore, complex background fluorescence and other experimental artifacts make effective measurement noise difficult to predict and/or relate in a simple fashion to nominally detected photons.[27,56]

Linear SDE Model Considered. The specific model we consider is a linear SDE parametrized by a finite dimensional vector denoted by θ. The parameters contained in θ and the remaining terms in eqs 1 and 2 are defined by the following equations:

$$F(r) = A + Br \tag{3}$$

$$\sigma = C \tag{4}$$

$$\Phi = \sigma\sigma^T/k_BT \tag{5}$$

$$\varepsilon \sim \mathcal{N}(0, R) \tag{6}$$

The collection of parameters to be estimated by the data will be denoted by $\theta \equiv (A,B,C,R)$. A is a 3D vector (i.e., $A \in \mathbb{R}^3$). B, C, and R are 3×3 real matrices.

Physical Interpretation of the SDE Model Parameters. The equations above were inspired by models in statistical physics.[49,53] For example, k_BT represents Boltzmann's constant multiplied by the system temperature. The fitted SDE is used to infer physical information about dynamical processes acting on the tagged particle, e.g., $F(r_t)$ denotes the effective force acting on the particle implied by the observations. A quantity like $F(r_t)$ contains information about how the local cellular environment is affecting the tagged particle. The parameter $C = \sigma$ determines the local diffusion[53] matrix defined by the relation $D \equiv \sigma\sigma^T$ (i.e., σ is the Cholesky factor of D). Inertia of the particle is ignored through a fluctuation dissipation relationship stated in eq 5, i.e., the tagged particle is in the "overdamped" regime;[53] Φ is a matrix quantifying effective friction (inducing the "overdamping"). The instantaneous velocity of the overdamped particle is quantified by $\Phi F(r_t)$. B can be interpreted as an elasticity parameter. We later check the modeling assumptions (e.g., overdamped regime and Brownian noise) against experimental data.[43]

Time Window-Based Parameter Estimation and Testing. Parameters approximating the dynamics or measurement statistics of the tagged particle change in an effective continuous fashion with time in many SPT applications. In all cases analyzed, the tagged particle measurement noise changed smoothly over the course of one trajectory. If a fixed constant measurement noise for single a SPT trajectory was assumed, this would be enough to cause model rejection by the goodness-of-fit hypothesis tests employed (see Figures S8 and S9, Table S1, and associated SI discussion). Motivated by the fact that parameters characterizing the dynamics and measurement noise change over time, we subdivide each trajectory into K blocks of contiguous time windows. In each window, we fit the parameters of an SDE to each of the following time series: $\{\psi_{t_i}\}_{i=n_0}^{n_1}$, $\{\psi_{t_i}\}_{i=n_1}^{n_2}$..., $\{\psi_{t_i}\}_{i=n_{K-1}}^{n_{K=N}}$ The inferred information from a single trajectory is summarized in K parameter vectors: $\theta^{(1)}$, $\theta^{(2)}$, ...$\theta^{(K)}$.

We force the value of the differences $W \equiv (n_{i+1} - n_i) + 1$ representing the number of observations in a given local time window to be a constant value. The term "micro-time" is used to refer to the times within local windows. For example, in local time window 2, we have the observations $\{\psi_{t_i}\}_{i=n_1}^{n_2}$ indexed by the micro-times t_{n1}, t_{n1+1}, ..., t_{n2}; the time-ordered sequence is subsequently used to infer the SDE parameter vector $\theta^{(2)}$. The local time window is independent of the volume traversed by the particle. This was done in order to keep the time series sample sizes the same and hence facilitate comparing goodness-of-fit test statistics coming from each window (i.e., the number of experimental observations used to scrutinize model predictions is the same in each local window).

In this article, we restrict our attention to the 3D linear SDE model described earlier because this model can be fit via maximum likelihood methods using quantities associated with the Kalman filter.[57] The Kalman filter is well-established[58] and has been used in SPT analyses.[35,59−62] Details outlining how MLE and the likelihood can be extracted from the linear model are contained in the SI.

Even though the likelihood of the measurement sequence can be computed exactly under the Kalman filter, goodness-of-fit tests simultaneously checking all distributional assumptions

dx.doi.org/10.1021/jp4064214 | J. Phys. Chem. B 2013, 117, 15701−15713

Table 1. Parameter Estimates for 3D Simulation Data[a]

case	1	2	3	4	truth
A_x	−0.003 (0.008)	−0.000 (0.006)	0.000 (0.003)	0.001 (0.002)	0
A_y	0.003 (0.015)	−0.000 (0.007)	0.000 (0.009)	−0.000 (0.001)	0
A_z	0.003 (0.031)	−0.001 (0.004)	0.009 (0.014)	−0.001 (0.004)	0
B_{xx}	−10.735 (3.236)	−3.896 (0.889)	−9.790 (1.138)	−3.586 (0.556)	−10
B_{xy}	10.542 (3.267)	-	9.825 (1.442)	-	10
B_{xz}	−0.597 (3.080)	-	−0.140 (1.941)	-	0
B_{yy}	−16.319 (4.071)	−5.879 (1.245)	−15.190 (2.005)	−5.397 (0.519)	−15
B_{yz}	1.049 (2.959)	-	0.351 (1.807)	-	0
B_{zz}	−45.543 (14.190)	−42.906 (11.842)	−43.790 (4.924)	−42.353 (4.107)	−40
C_x	0.209 (0.050)	0.159 (0.025)	0.209 (0.012)	0.157 (0.007)	0.2
C_y	0.148 (0.028)	0.121 (0.016)	0.143 (0.016)	0.119 (0.009)	0.15
C_z	0.103 (0.033)	0.106 (0.042)	0.095 (0.015)	0.098 (0.015)	0.10
R_x	0.020 (0.002)	0.021 (0.001)	0.020 (0.001)	0.021 (0.001)	0.020
R_y	0.015 (0.001)	0.016 (0.001)	0.015 (0.001)	0.016 (0.001)	0.015
R_z	0.010 (0.002)	0.010 (0.002)	0.010 (0.001)	0.010 (0.001)	0.010

[a]In each case, a time series consisting of 1×10^5 observations uniformly spaced by 4 ms was simulated to create draws from the stationary distribution of a 3D model. Parameters were estimated by dividing the long stationary signal into windows using various schemes. Case 1: Computed average and standard deviation (reported in parentheses) of 3D model estimated with 400 observations per window. Case 2: Results with 1D model estimated with 400 observations (interaction terms B_{xy},B_{xz},B_{yz} are set to zero). Case 3 and 4: Correspond to Case 1 and 2 except using a window of size 1600 (resulting in a larger sample size for each parameter estimate).

were difficult to rigorously address before the advent of recent advances in time series analysis.[43−45,47] The aforementioned approaches have been utilized extensively in scalar time series, but statistical inference in the multivariate nonstationary case is currently an open problem.[45,47] A brief description of the tests used here[43] are provided in the next subsection; a more detailed discussion is contained in the SI Theory and Methods section where we discuss how the technical difficulties associated with the multivariate version of Hong and Li's test[43] are addressed (advantages over traditional Kalman filter techniques are also provided in the SI, e.g., see Figure S9 and associated discussion).

Throughout, we also restrict attention to the case where C and R are diagonal (uncorrelated thermal and measurement noise) and $F(r)$ comes from the gradient of a scalar potential (hence B is symmetric). It should be noted that one can also consider nongradient forces and/or nonlinear multivariate SDEs in both estimation[53,63] and inference;[43,45] we focus on the linear case described above to simplify exposition. In the cases rejected in this Article, using nonlinear polynomial SDE models did not improve the model fit (quantified in next section).

EXPERIMENTAL METHODS

Sample Preparation and Microscopy. A time-ordered image stack where consecutive images were measured every 4 ms was used to generate each SPT trajectory. Sixty *ARG3* mRNA trajectories in budding yeast visualized by EGFP fusions to proteins binding MS2 loop repeats were analyzed in total at this sampling frequency. 3D measurements were obtained by analyzing a double-helix point spread function (DH-PSF)[8,10,64] response in each image. The experimental setup and data processing method used are described in Thompson et al.[10] The mRNA trajectory extracted from the image stack was divided into contiguous windows each containing $W = 400$ noisy 3D observations (the number of contiguous observations was determined to provide a balance between variance and bias). The results reported were not found to depend on the window size or the temporal sampling rate (see SI). Using $W = 400$ resulted in a total of 473 windows of 3D data. Individual single particle trajectories were associated with $K = 4-12$ blocks of local window data. The length of data associated with one trajectory depended stochastically on photobleaching effects.

Signal Processing. Initially, we assumed that the three position coordinates evolved statistically independently of one another when estimating the SDE parameters in the 473 windows of 3D data. The assumption of statistical independence of the position coordinates effectively increased the number of 1D SDE parameter vectors estimated to $1419 = 3 \times 473$. In the 3D cases considered, the total number of parameters to estimate for each trajectory is 15 in the 3D SDE models considered.

Local MLE of 3D Trajectories. Estimation of the parameters in local window j was achieved by recording the measurements at W micro-times and using them to obtain the MLE defined by:

$$\hat{\theta}^{(j)} = \operatorname{argmax} l(\theta^{(j)}) \tag{7}$$

$$l(\theta^{(j)}) \equiv \sum_{i=n_{j-1}+1}^{n_j} \log(p(\psi_{t_i}|\psi_{t_{i-1}}; \theta^{(j)}))$$

where the parameter vector $\hat{\theta}^{(j)} \equiv (\hat{A},\hat{B},\hat{C},\hat{R})$ is the MLE assuming the initial measurement is precisely known.[57] Finding the MLE requires one to evaluate the transition density, $p(\psi_{ti}|\psi_{ti-1};\theta^{(j)})$. In the Kalman filter case considered, the transition density is a multivariate Gaussian density. The SI contains the equations connecting the continuous time SDE to the discrete Kalman filter,[57] as well as details of initial parameter guesses and goodness-of-fit statistics. Throughout, we focus on $W = 400$, but other values are explored in the SI.

Hypothesis Testing Procedure. After fitting models to observed experimental data, we used the MLE to form the "null hypothesis"[43] and computed two test statistics: (1) the omnibus "Q-test" introduced by Hong and Li;[43] this test statistic simultaneously checks the distributional shape and the statistical dependence in the probability integral transform

dx.doi.org/10.1021/jp4064214 | J. Phys. Chem. B 2013, 117, 15701−15713

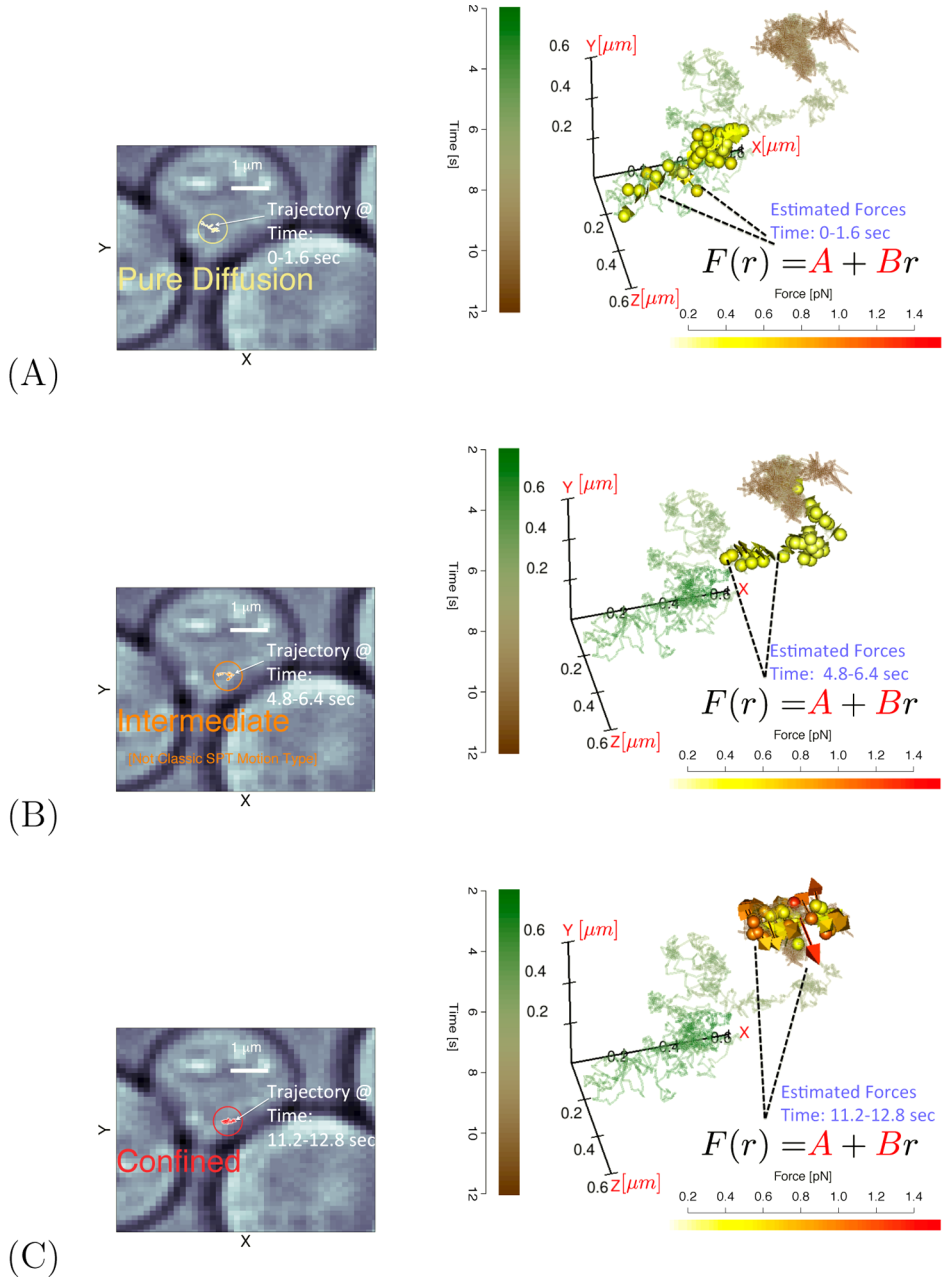

Figure 1. The left column panels display 2D segments of a single mRNA trajectory for three different time windows. The right panels repeatedly plot the full 3D trajectory as a solid line (time color coded); in each panel, the inferred force vectors corresponding to the time segments shown the 2D panel to the left are plotted (force magnitude color code shown in scale bar). These forces were obtained by first estimating the SDE parameters in the window and then using the measurements to evaluate the force at several "micro-times" in the local time window. Panel A corresponds to the force estimated in window 1; this panel would be typically labeled as a "pure diffusion" as the force vectors estimated are very small. Panel B corresponds to time window 4 where there is a transient regime that would not fall into any classical single particle tracking motion type. Panel C plots time window 8 data which would be considered as "confined". The inferred force vectors can be estimated from the observed time series without using an external force probe; the magnitude and direction of the forces arrows help identify the inward facing forces experienced by the confined particle. All 3D images were produced using the RGL package.[65]

(PIT), and (2) the "M-test".[43] The latter focuses only on statistical dependence in the computed PIT sequence. More specifically, the name "M-test" is used to refer to M(1,1)[43] with a lag truncation parameter of 20; in this study, results obtained using $M(i,j)$ were similar for $i,j \in \{1,2\}$ and lag parameters of 10 and 30. We used the sampling parameters $j = 1$ and $p = 20$[43] to construct the Q test statistic, but our findings supported those reported in Hong and Li.[43] That is, the M and Q test results are effectively independent of sampling parameters.

For the Kalman filter model, the PIT sequence (required for the tests mentioned above) was computed using the normalized innovation sequence (i.e., the innovation vector multiplied by the inverse matrix square root of the innovation covariance) using the observed data and the fitted $\hat{\theta}^{(j)}$. Note that this approach uses a linear combination of 3D elements and aims at removing empirical correlation between observations; this partially mitigates issues associated with computing the PIT of a multivariate time series.[43]

dx.doi.org/10.1021/jp4064214 | J. Phys. Chem. B 2013, 117, 15701−15713

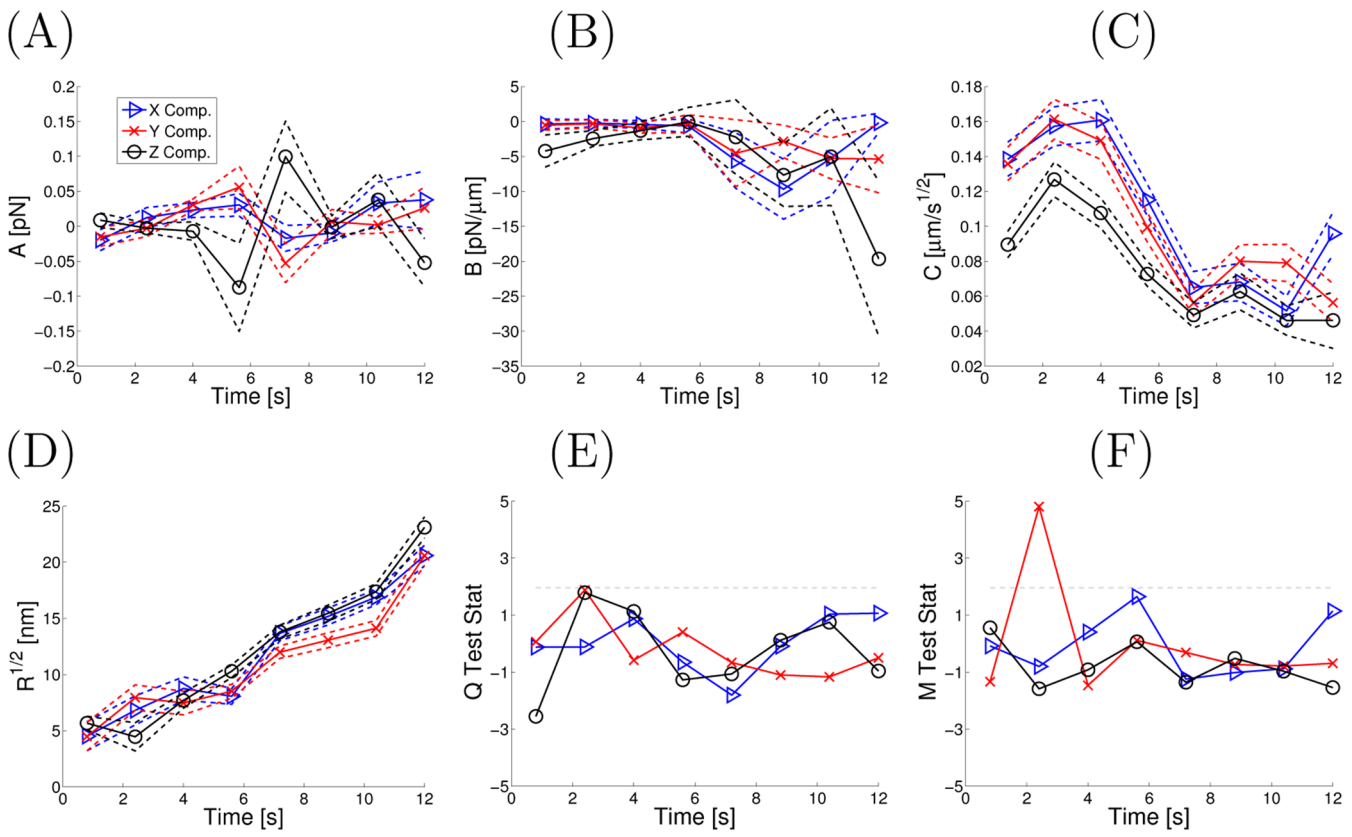

Figure 2. Parameters of time windowed SDEs estimated from experimental data. Panels A–D show SDE parameters corresponding to Figure 1; the solid lines connect the parameters estimated in the different windows, and the dashed lines correspond to the standard deviation (parameter uncertainty) associated with a simulated SDE possessing the same parameters as those observed for the experimental data. Panels E and F plot two test statistics used in assessing the fit of the assumed SDE model given the observational data. The results shown are for a case where traditional SPT models were not rejected (hence the off-diagonal terms in B are set to zero).

Computing Error Bars. Finite time series sample sizes introduce inherent parameter uncertainty into the estimates. If an SDE is fitted, and the goodness-of-fit test suggests that there is no evidence of inconsistency between the model and data, then we turn to Monte Carlo Simulations for extracting error bars. The point MLE is used to generated multiple synthetic trajectories (each having the same number of observations as the experimental data); subsequently, the MLE of each synthetic path is extracted. From this collection of estimated parameters, the standard error, SE, of each element of $\hat{\theta}^{(j)}$ is extracted, and the range of plausible parameters is approximated by $\hat{\theta}^{(j)} \pm \mathrm{SE}$.

RESULTS AND DISCUSSION

Control Simulations. To begin, we start with a situation where a 3D SDE simulation is used to generate data (i.e., measurement noise with precisely known statistics was added to the synthetic observations). The parameters were forced to be fixed for the duration of the simulation and the interest is in quantifying how accurately parameters describing x,y,z force interactions can be characterized under a correctly and incorrectly specified model with simulation parameters selected to mock experimental conditions. Table 1 reports the mean and standard deviation of these parameters (see caption for additional Monte Carlo simulation details). The last column of Table 1 provides the parameter of the underlying true data generating model; the first and third columns present parameter estimation results using the 3D SDE model proposed (the columns differ in the number of temporal observations used for each MLE estimate); the second and fourth columns present results obtained by a "classic 1D SPT" model where interaction terms (e.g., B_{xy}) are set to zero. Note that parameter estimates for the classic 1D SPT induce appreciable bias in both the "elasticity" parameters (components of B) and the diffusion coefficient. These results indicate that using a time series size of $W = 400$ has power to detect 3D force interaction terms in the sample sizes and observation frequencies studied. Table S4 provides additional evidence that the method has adequate power to detect kinetic phenomena of interest in the experimental mRNA trajectories.

Estimation of SPT Models with Time Varying Parameters. Here we first consider an actual experimental case of motion of a single mRNA particle in a cell where the assumption of statistical independence between the coordinates was not rejected by the goodness-of-fit tests employed. Figure 1 presents three panels where the entire noisily measured trajectory (containing both thermal and measurement noise) is plotted, and the behavior during time windows 1, 4, and 8 are highlighted. Superimposed, the inferred forces at different micro-times are plotted as colored arrows in the three panels; in case A the force vectors are so short that only the yellow tails of the force vectors are visible.

It is possible that a single tagged particle tracked for a long enough time can exhibit a dynamical regime change.[29,66] For example, the particle can change from exhibiting "pure" diffusion to one consistent with another mode of motion

dx.doi.org/10.1021/jp4064214 | J. Phys. Chem. B 2013, 117, 15701–15713

such as "directed motion" or "corralled/confined" diffusion.[16,29,66] We clearly observe regime changes in this single trajectory; for example, window 1 (Figure 1A) would be considered a "pure diffusion" regime, whereas window 8 (Figure 1C) would likely be classified as "corralled diffusion".[29] However, window 3 (Figure 1B) would not cleanly fit into any classic SPT motion model (it is intermediate between diffusive and corralled). The change between the two regimes is relatively smooth and slow relative to the temporal sampling frequency. The inferred vectors quantify the magnitude and direction of the forces acting on the particle in the corralled/confined region. A discussion comparing and contrasting the type of corralled/confined diffusion model considered here to other classical confinement models[15,17] is presented in ref 67.

Figure 2 presents more quantitative results illustrating that the particle shown in Figure 1 is experiencing smooth changes in the SDE parameters. In Figure 2A, we plot the estimated $\hat{A}$ (see Methods) versus time. The dashed lines corresponds to parameter uncertainty in the estimate. The confidence bands were obtained via Monte Carlo simulation techniques outlined in the Methods. Panels B−D are similar except they correspond to the parameters $\hat{B}$, $\hat{C}$ and $\hat{R}$, respectively. Regarding potential physical interpretation, the time varying $\hat{C}$ can correspond to the mRNA−protein (mRNP) complex changing its effective hydrodynamic radius in a nontrivial fashion as it traverses the cell; the increase in magnitude of $\hat{B}$ can be explained by a tagged mRNP aggregate slowly binding to a larger physical object in the cytoplasm. However, both of these explanations require additional studies (e.g., multicolor SPT experiments) to verify the posited interpretations since the effective diffusion coefficient and elasticity can change for other reasons, such as changes in local viscosity or other factors.[53] The time dependence of $\hat{R}$ showing increasing measurement noise (increasing uncertainty in position) is far less ambiguous since multiple GFPs are attached to the mRNA;[10] the decay in intensity is caused mainly by different dyes photobleaching at different random times, and this reduces the experimenter's ability to extract precise positions.

Figure 2 also demonstrates that the change in dynamical responses is not instantaneous on time scales now resolvable in single-molecule experiments (a pure diffusion continuously morphs into a corralled diffusion). Figure S6 demonstrates that parameter estimates obtained by analyzing the experimental mRNA SPT data are insensitive to the sampling parameter W and the time between successive observations. Panels E and F in Figure 2 plot the Q and M goodness-of-fit statistics associated with the observed data and the estimated $\theta^{(j)}$. The dashed lines in panels E and F denote the asymptotic critical values of the Q and M test statistics; test statistic values above this threshold indicate a fitted model inconsistent with the observed data with an asymptotic one-sided significance level (without multiple testing correction) of 2.5%.

SDEs with smoothly evolving parameters was a common feature in this mRNA SPT data. For example, in all observed trajectories, the effective measurement noise was observed to smoothly vary over the course of data collection, and the change within individual trajectories was statistically significant (see Figure S4). Parameters characterizing particle motion smoothly changing over time has important implications in regards to explaining causes of anomalous diffusion[14,22,31,68,69] and for tracking groups of particles in the cytoplasm where dynamical models (with fixed parameters) are often utilized.[35,59−62]

The SI (Figure S5 and Tables S1−S3) displays some problems that can occur if one does not account for time-varying parameters in classic SPT analysis methods. Traditional models estimated by MLE assume fixed parameters or impose heuristics for truncating trajectories, e.g.;[10,16] if the underlying data changes appreciably, then significant biases can be introduced. Worse yet, large transient forces of physical interest may go unnoticed (e.g., as shown in the next subsections). Tables S1 and S3 show that the testing procedure employed can quantitatively determine whether there is adequate evidence in the data to detect time changing parameters in one trajectory. Figure S5 provides results analogous to Figure 2, where a windowing approach is used in conjunction with the MSD estimator utilized in ref 10. It can be observed that bias and variance of a commonly used MSD method is substantial, even if local time windows are used with the MSD estimator. Figure S5 also shows that for this trajectory (with time-changing SDE parameters), the bias is most substantial in the estimated effective measurement noise (this parameter is also known as the effective localization precision).

In the Experimental Methods, we discussed how an initial screening of 1419 1D models was carried out. In this data set, 136/1419 1D SDE models were rejected by the Q-test, and 290/1419 were rejected by the M-test[43] using a test statistic threshold corresponding to the critical value where 97.5% of the standard Normal probability mass is less than the threshold value. The initial screening was done in order to reduce the computational load associated with fitting a large batch of 3D SDE models. After further inspection of the rejected cases, it was found that several trajectories where 1D SDE models assuming independently evolving coordinates were rejected exhibited rich dynamics (some examples are presented in the sections that follow; other examples can be found in the Figures S2−S4). Of the trajectories rejected, inclusion of a 3D force permitting coupling between the x,y,z, forces in the SDE improved the fit in terms of the Akaike information criterion (AIC) and Bayes information criterion (BIC) model selection criteria and/or goodness-of-fit. Note that increasing the polynomial order of the SDE, producing a 3D analogue of the nonlinear SDE model utilized in ref 21 did not improve the fit; the M-test only rejected 266/1419, whereas the linear Kalman filter performed similarly (290/1419).

Note that the models considered do not explicitly account for a single-ended hard boundary (e.g., a cell wall). If the wall is static and the particle continually strikes a single-ended boundary, this modeling imperfection will likely be detected by the goodness-of-fit tests. The reason for rejection would not be provided, but additional diagnostic analyses would likely show that a region of occluded phase space is visited less frequently than the assumed model predicts it should. In general, if the particle has an affinity for a singled-ended boundary and it hits this boundary often on the experimental time scale, another model should be considered. In systems we have encountered, 2−4 "hard" reflections in a time series of size 200−400 hitting a (nominally) known physical barrier have not adversely affected estimation or goodness-of-fit testing. Effects of two-ended boundaries (with hard or soft repulsions) have been recently analyzed by the first author;[67] in this work, the focus was on studying short SPT trajectories (100−400 observations) containing thermal and measurement noise. The work in ref 67 complements the study provided in ref 18 where long (>4000) trajectories were analyzed.

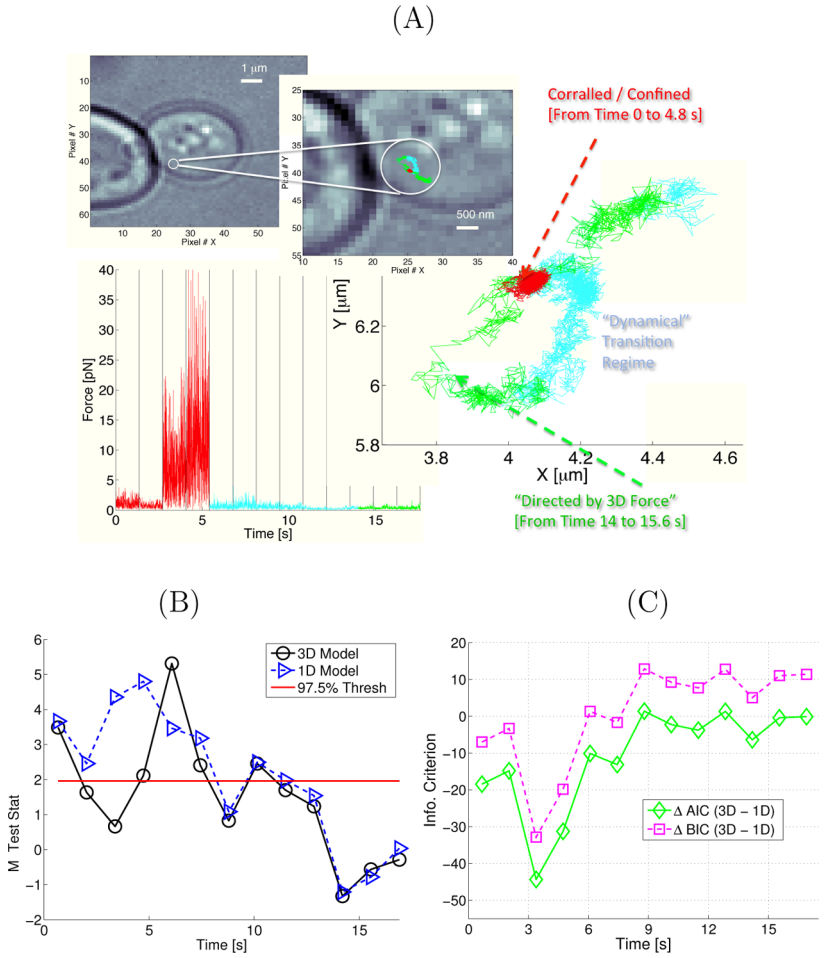

Figure 3. A case where the particle interacts with an object in the cytoplasm. Panel A shows the location in the cell where the image was taken. The microscope images is magnified, and the $x-y$ coordinates of the experimentally measured trajectory are shown in color. The red region shows where the particle was confined by large constraint forces. The inferred forces reached magnitudes as high as 30pN for long time bursts (Figure S7 illustrates that this force burst was insensitive to W); the cyan region is a dynamical regime encountered before the particle experiences a "3D directed force" (a regime denoted by green and discussed in the text). Panel B plots the goodness-of-fit test statistic, and panel C plots the AIC and BIC comparing a genuine 3D model to a 1D model (lower values indicate better fits for both goodness-of-fit and model selection statistics). The trajectory strongly suggests constraint forces and the AIC and BIC model selection criteria verified that adding correlation between the effective forces governing the particle dynamics improves the fit. The experimental trajectory and effective forces imply the existence of a manifold on which the particle evolves. The SDE quantifies the strength of the "tether" to this manifold.

Discoveries Enabled via Goodness-of-Fit Tests. Next, we demonstrate another case where a dynamical regime change was observed along a single 3D trajectory. Importantly, this trajectory was flagged by the goodness-of-fit test as not being consistent with three independent traditional 1D SPT models. The white light image of the cell containing the tagged particle is shown in Figure 3A. The 2D projection of the measured 3D DH-PSF trajectory is shown in the white light image magnification displayed in Figure 3A. The 2D projection is color-coded by a loose qualitative regime labeling we applied to the data after analysis of the implied force magnitudes (these regimes are discussed more in subsequent sections). The 3D force magnitude was inferred from $K = 13$ windows. The window boundaries are indicated by vertical lines in the bottom left plot of panel A. The red label denotes the confined regime where the particle was observed to exhibit large bursts of force ranging from 1 to 30 pN. Figure S7 demonstrates that the force bursts were not overly dependent on the sampling parameter W. Note that the elasticity inferred during the force burst (e.g., 650.4−975.6 pN/μm in z) is much larger than standard RNA elasticities reported in the literature[70,71] and the size of the force magnitude is consistent with those forces studied via in vitro ribosome/mRNA studies.[72,73] Figure 3B presents the M test statistic, which indicates superior performance from a 3D model during the confinement period. Figure 3C demonstrate quantitatively that the 3D SDE model also improves performance in terms of the AIC and BIC[54] model selection criteria (a value less than zero in Figure 3C suggests a 3D model is preferred by the model selection criteria). The green region shown in Figure 3A is a "directed by 3D force regime". By this we mean that an SDE model allowing for statistically correlated 3D forces was used, i.e., the elasticity matrix had statistically significant terms in the off-diagonal entries (as determined by AIC and the inferred force arrows).

Figure 4 plots the raw 3D trajectory (i.e., the full information afforded by the DH-PSF measurements) as well as the inferred forces in the two different regimes (these regimes were highlighted in Figure 3A). Figure 4A displays a confined regime where the tagged particle experiences equal and opposite forces pointing in spatial directions indicated by the force vectors.

dx.doi.org/10.1021/jp4064214 | J. Phys. Chem. B 2013, 117, 15701−15713

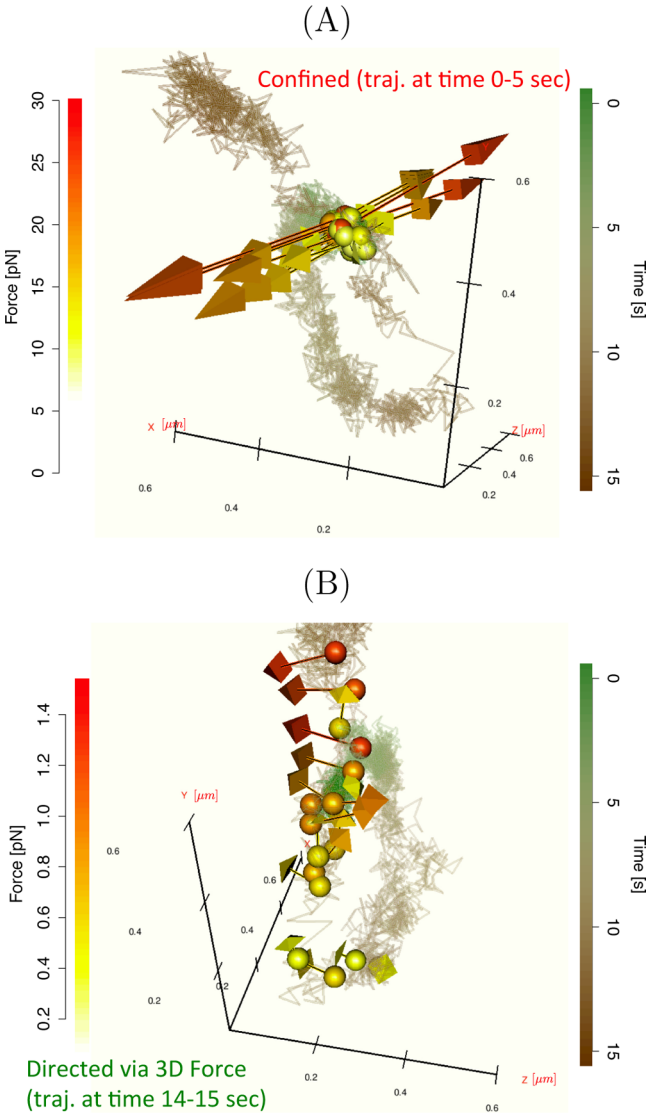

Figure 4. Inferred force vectors for the trajectory in Figure 3. The solid lines show the 3D measurements, and the colored spheres and arrows denote the inferred 3D force vector. Panel A plots representative forces associated with the confined motion regime, and panel B shows those associated with the directed regime.

Figure 4B shows, after an intermediate transition time occurring between seconds 5 and 14, that the type of dynamics the tagged particle experiences changes during time 14−15 s. The tagged particle experiences statistically significant constraint forces during time 14−15 s. In this regime, the SDE model selection analysis (see Figure 3C) suggests that the sequence of measurements is best explained by forces whose components are statistically dependent.

Some possible physical interpretations of the dynamical transitions described above are posited in the text below. In the confined regime (Figure 4A), the mRNA particle appears to be tightly bound to another molecule. After this binding, the dynamics experienced by the particle slowly change into forces suggesting that the mRNA complex engages in active transport (Figure 4B). In the active transport regime (Figure 4B), the mRNP complex appears to be tethered to a cytoskeletal track (e.g., a microtubule or actin cable) and subsequently shuttled (i.e., directed) by 3D forces plotted in Figure 4B. The estimated 3D forces are described in greater detail in the next subsection.

Another, albeit more ambitious, interpretation of this data is that the observed phenomenon is a dynamical signature associated with the translation of mRNA by a ribosome.[72,74,75] The force magnitudes inferred by the SDE are in the 1−30 pN range for bursts; this range can possibly be explained by ribosomal forces;[72] however, our experiments are different in spirit (namely, the fluorescently tagged molecule is being "passively" observed in vivo) so directly comparing force magnitudes is not straightforward. However, further research is needed to determine what would cause the constrained motion observed (e.g., techniques able to resolve both mRNA and a binding ribosome with high spatial and temporal resolution are needed, such as two color imaging). The ribosome interpretation is admittedly ambitious, but the highly directed inferred force vectors are nonetheless useful in determining that the particle is interacting strongly with another object in the cytoplasm. This discovery was enabled by goodness-of-fit tests identifying inconsistencies of the SPT data with traditional SPT models.

New Kinetic Signatures of in Vivo Transport. Typically, a mean square displacement analysis coupled with a large measured velocity characterizes directed motion. However, both the velocity magnitude and duration of directed motion on cytoskeletal structures in cells are difficult to reliably quantify at the single-molecule level.[10,29] The use of inferred SDE forces evaluated for each SPT measurement in-hand can help in providing another dynamical fingerprint of directed transport along a cytoskeletal track.

Regarding the experimental system under study, molecular motors are believed to shuttle mRNP complexes in yeast cells.[29] When a mRNP complex is moved by a motor along a track, a force must act tangential along the track in order for "directed transport" to occur, but other forces must also be involved. For example, a motor stalk must tether the cargo near the track. The force vectors observed in Figure 4B are suggestive of both a classic directed force (the force arrows point in a common direction) and a tethering force constraining the mRNP near a cytoskeletal track (this induces forces "orthogonal" to the direction of motion). The implied SDE forces just described thus display a 3D pattern as opposed to a 1D pattern typically used to characterize directed motion in SPT studies. The velocity of the directed transport observed in this trajectory reached an average value of 490 nm/s in the directed regime. This magnitude is not excessively large but coupled with the force vector magnitude and directionality (suggesting a tethering force), the possibility of the tagged mRNP being shuttled across the cytoskeletal highway seems more plausible.

To classify the motion of all trajectory segments studied in the spirit of traditional SPT literature, four 1D model types were estimated via MLE. In other sections, we did not need to select a category for the dynamics (SDE parameters were simply estimated; then the statistical significance and physical interpretation of model parameters can be determined *a posteriori*), but to assign categories to all trajectories and compare to other published literature classifications, we selected the model type using the simplest model not rejected by the Q test. For example, a trajectory would be labeled "static" if the goodness-of-fit test failed to reject a model whose only nonzero MLE parameters were contained in $\hat{R}$. Using this approach, the fraction of trajectory segments identified to be undergoing 1D directed motion (≈ 6.7%) and "static motion" (≈ 28.1%) is comparable to previously published literature

dx.doi.org/10.1021/jp4064214 | J. Phys. Chem. B 2013, 117, 15701−15713

values.[29] In the work of Fusco et al.[29] another "housekeeping" mRNA was studied; the fractions of trajectories reported to experience directed motion was ≈3.0%, and those considered static were ≈31.0%. We compared these two motion types because unambiguously distinguishing between other motion types can be even more subjective.[10,29]

CONCLUSIONS

We have demonstrated how likelihood-based statistical inference can lead to new quantitative insights about complex biological processes in live cells. Our methods were able to quantify the 3D forces associated with tagged mRNA interacting with cellular structures in yeast. The goodness-of-fit tools coupled with the multidimensional SDE estimation methods provided strong evidence of the tagged particle interacting with other components in the cytoplasm. Accurately quantifying the time evolving measurement and thermal noise was crucial in the success of this endeavor. The statistical diagnostics tested whether the various assumptions implicit in our model (e.g., local linear overdamped forces and Gaussian measurement noise) were justified given the data. It is known that distinguishing between pure diffusion, corralled/confined diffusion, and a "static" particle is a difficult and mildly subjective task;[16,29] fortunately, our models can be applied without assuming a subjective label. The only subjective information assumed was the parametric model form, but we used the goodness-of-fit tests to check our assumptions (with single-molecule precision) against experimental data.

Many interesting 3D forces were only uncovered because of the statistical rejection of classic SPT diffusion models by the goodness-of-fit tests employed.[43] Without the use of new goodness-of-fit tests capable of simultaneously testing all distributional assumptions (properly accounting for inherent thermal and measurement noise and also able to measure inconsistencies in assumed velocity or force) along a single trajectory, these interesting scientific results would have been missed due to the volume of trajectory data produced. The unusual number of statistical rejections along a subset of trajectories flagged some dynamically unusual trajectories and inspired additional investigation. New kinetic signatures of directed motion and binding were suggested when classic SPT models were rejected. Kinetic signatures not depending on (relatively) long-lived large constant velocity can assist in identifying both "traditional directed transport" and "tug-of-war" type forces acting on a tagged particle.[76,77] Utilizing and expanding on recent advances in rigorous time series analysis[43−47] shows promise in SPT applications where dynamical models required by linear or nonlinear tracking tools need to be systematically checked. It should be stressed that the goodness-of-fit testing approach used here[43] is readily applicable to local nonlinear SDEs and other more complex stochastic models.[20,36,53] Examples of other trajectories exhibiting directed transport and forces discovered by the goodness-of-fit screening can be found in Figures S1−S3.

ASSOCIATED CONTENT

Supporting Information

A PDF containing extra simulation and experimental results (with table of contents). This material is available free of charge via the Internet at http://pubs.acs.org.

AUTHOR INFORMATION

Corresponding Authors

*E-mail: chris.calderon@numerica.us. Mailing address: Numerica Corporation, Loveland, CO 80538, U.S.A. Tel.: (970) 612-2336. Fax: (970) 461-2004.

*E-mail: wmoerner@stanford.edu.

Present Addresses

[‖]3308 Langley Ct., Flower Mound, TX 75022.

[⊥]Solazyme, Inc., 225 Gateway Boulevard, South San Francisco, CA 94080.

Notes

The authors declare no competing financial interest.

ACKNOWLEDGMENTS

The authors would like to thank Prof. Patrick Brown for useful discussions related to this work and Dr. Bryon Donohoe for providing comments on a draft of the manuscript. C.P.C. and R.C.P. were funded by internal R&D funds provided by Numerica Corporation; W.E.M. was supported by a grant from the National Institute of General Medical Sciences (R01GM085437).

REFERENCES

(1) Arhel, N.; Genovesio, A.; Kim, K.; Miko, S.; Perret, E.; Olivo-Marin, J.; Shorte, S.; Charneau, P. Quantitative Four-Dimensional Tracking of Cytoplasmic and Nuclear HIV-1 Complexes. *Nat. Methods* **2006**, *3*, 817−824.

(2) Brandenburg, B.; Zhuang, X. Virus Trafficking - Learning from Single-Virus Tracking. *Nat. Rev.: Microbiol.* **2007**, *5*, 197−208.

(3) Lessard, G. A.; Goodwin, P. M.; Werner, J. H. Three-Dimensional Tracking of Individual Quantum Dots. *Appl. Phys. Lett.* **2007**, *91*, 224106.

(4) Nägerl, U. V.; Willig, K. I.; Hein, B.; Hell, S. W.; Bonhoeffer, T. Live-Cell Imaging of Dendritic Spines by STED Microscopy. *Proc. Natl. Acad. Sci. U.S.A.* **2008**, *105*, 18982−7.

(5) Huang, B.; Wang, W.; Bates, M.; Zhuang, X. Three-Dimensional Super-Resolution Imaging by Stochastic Optical Reconstruction Microscopy. *Science* **2008**, *319*, 810−813.

(6) Rohatgi, R.; Milenkovic, L.; Scott, M. P. Patched1 Regulates Hedgehog Signaling at the Primary Cilium. *Science (New York, N.Y.)* **2007**, *317*, 372−6.

(7) Manley, S.; Gillette, J.; Patterson, G.; Shroff, H.; Hess, H.; Betzig, E.; Lippincott-Schwartz, J. High-Density Mapping of Single-Molecule Trajectories with Photoactivated Localization Microscopy. *Nat. Methods* **2008**, *5*, 155−157.

(8) Pavani, S. R. P.; Thompson, M. A.; Biteen, J. S.; Lord, S. J.; Liu, N.; Twieg, R. J.; Piestun, R.; Moerner, W. E. Three-Dimensional, Single-Molecule Fluorescence Imaging Beyond the Diffraction Limit by Using a Double-Helix Point Spread Function. *Proc. Natl. Acad. Sci. U.S.A.* **2009**, *106*, 2995−9.

(9) Rohatgi, R.; Milenkovic, L.; Corcoran, R. B.; Scott, M. P. Hedgehog Signal Transduction by Smoothened: Pharmacologic Evidence for a 2-Step Activation Process. *Proc. Natl. Acad. Sci. U.S.A.* **2009**, *106*, 3196−201.

(10) Thompson, M. A.; Casolari, J. M.; Badieirostami, M.; Brown, P. O.; Moerner, W. E. Three-Dimensional Tracking of Single mRNA Particles in *Saccharomyces cerevisiae* Using a Double-Helix Point Spread Function. *Proc. Natl. Acad. Sci. U.S.A.* **2010**, *107*, 17864−71.

(11) Sahl, S. J.; Leutenegger, M.; Hilbert, M.; Hell, S. W.; Eggeling, C. Fast Molecular Tracking Maps Nanoscale Dynamics of Plasma Membrane Lipids. *Proc. Natl. Acad. Sci. U.S.A.* **2010**, *107*, 6829−34.

(12) Grünwald, D.; Singer, R. H. In Vivo Imaging of Labelled Endogenous β-Actin mRNA During Nucleocytoplasmic Transport. *Nature* **2010**, *467*, 604−609.

(13) Lange, S.; Katayama, Y.; Schmid, M.; Burkacky, O.; Bräuchle, C.; Lamb, D. C.; Jansen, R.-P. Simultaneous Transport of Different

Localized mRNA Species Revealed by Live-Cell Imaging. *Traffic (Copenhagen, Denmark)* **2008**, *9*, 1256−67.
(14) Qian, H.; Sheetz, M. P.; Elson, E. L. Single Particle Tracking. Analysis of Diffusion and Flow in Two-Dimensional Systems. *Biophys. J.* **1991**, *60*, 910−21.
(15) Kusumi, A.; Sako, Y.; Yamamoto, M. Confined Lateral Diffusion of Membrane Receptors as Studied by Single Particle Tracking (Nanovid Microscopy). Effects of Calcium-Induced Differentiation in Cultured Epithelial Cells. *Biophys. J.* **1993**, *65*, 2021−40.
(16) Saxton, M. J.; Jacobson, K. Single-Particle Tracking: Applications to Membrane Dynamics. *Annu. Rev. Biophys. Biomol. Struct.* **1997**, *26*, 373−99.
(17) Kusumi, A.; Nakada, C.; Ritchie, K.; Murase, K.; Suzuki, K.; Murakoshi, H.; Kasai, R. S.; Kondo, J.; Fujiwara, T. Paradigm Shift of the Plasma Membrane Concept from the Two-Dimensional Continuum Fluid to the Partitioned Fluid: High-Speed Single-Molecule Tracking of Membrane Molecules. *Annual Rev. Biophys. Biomol. Struct.* **2005**, *34*, 351−78.
(18) Jin, S.; Haggie, P. M.; Verkman, a. S. Single-Particle Tracking of Membrane Protein Diffusion in a Potential: Simulation, Detection, and Application to Confined Diffusion of CFTR Cl- Channels. *Biophys. J.* **2007**, *93*, 1079−88.
(19) Savin, T.; Doyle, P. S. Static and Dynamic Errors in Particle Tracking Microrheology. *Biophys. J.* **2005**, *88*, 623−38.
(20) Calderon, C. P.; Chen, W.; Harris, N.; Lin, K.; Kiang, C. Quantifying DNA Melting Transitions Using Single-Molecule Force Spectroscopy. *J. Phys.: Condens. Matter* **2009**, *21*, 034114.
(21) Calderon, C. P.; Harris, N.; Kiang, C.; Cox, D. Analyzing Single-Molecule Manipulation Experiments. *J. Mol. Recognit.* **2009**, *22*, 356.
(22) Calderon, C. P. A Data-Driven Approach to Decomposing Complex Enzyme Kinetics. *Phys. Rev. E* **2009**, *80*, 061118.
(23) Michalet, X. Mean Square Displacement Analysis of Single-Particle Trajectories with Localization Error: Brownian Motion in an Isotropic Medium. *Phys. Rev. E* **2010**, *82*, 041914.
(24) Montiel, D.; Cang, H.; Yang, H. Quantitative Characterization of Changes in Dynamical Behavior for Single-Particle Tracking Studies. *J. Phys. Chem. B* **2006**, *110*, 19763−70.
(25) Voisinne, G.; Alexandrou, A.; Masson, J.-B. Quantifying Biomolecule Diffusivity Using an Optimal Bayesian Method. *Biophys. J.* **2010**, *98*, 596−605.
(26) Persson, F.; Lindén, M.; Unoson, C.; Elf, J. Extracting Intracellular Diffusive States and Transition Rates from Single-Molecule Tracking Data. *Nat. Methods* **2013**, *10*.
(27) Berglund, A. J. Statistics of Camera-Based Single-Particle Tracking. *Phys. Rev. E* **2010**, *82*, 011917.
(28) Michalet, X.; Berglund, A. Optimal Diffusion Coefficient Estimation in Single-Particle Tracking. *Phys. Rev. E* **2012**, *85*, 061916.
(29) Fusco, D.; Accornero, N.; Lavoie, B.; Shenoy, S. M.; Blanchard, J. M.; Singer, R. H.; Bertrand, E. Single mRNA Molecules Demonstrate Probabilistic Movement in Living Mammalian Cells. *Curr. Biol.* **2003**, *13*, 161−167.
(30) Feder, T.; Brust-Mascher, I.; Slattery, J.; Baird, B.; Webb, W. W. Constrained Diffusion or Immobile Fraction on Cell Surfaces: A New Interpretation. *Biophys. J.* **1996**, *70*, 2767−2773.
(31) Saxton, M. J. Single-Particle Tracking: The Distribution of Diffusion Coefficients. *Biophys. J.* **1997**, *72*, 1744−53.
(32) Magdziarz, M.; Klafter, J. Detecting Origins of Subdiffusion: P-Variation Test for Confined Systems. *Phys. Rev. E* **2010**, *82*, 011129.
(33) Burov, S.; Jeon, J.-H.; Metzler, R.; Barkai, E. Single Particle Tracking in Systems Showing Anomalous Diffusion: The Role of Weak Ergodicity Breaking. *Phys. Chem. Chem. Phys.* **2011**, *13*, 1800−12.
(34) Ensign, D. L.; Pande, V. S. Bayesian Detection of Intensity Changes in Single Molecule and Molecular Dynamics Trajectories. *J. Phys. Chem. B* **2010**, *114*, 280−92.
(35) Godinez, W. J.; Lampe, M.; Wörz, S.; Müller, B.; Eils, R.; Rohr, K. Deterministic and Probabilistic Approaches for Tracking Virus Particles in Time-Lapse Fluorescence Microscopy Image Sequences. *Med. Image Anal.* **2009**, *13*, 325−42.
(36) Calderon, C. P.; Harris, N.; Kiang, C.; Cox, D. Quantifying Multiscale Noise Sources in Single-Molecule Time Series. *J. Phys. Chem. B* **2009**, *113*, 138.
(37) Chenouard, N.; Dufour, A.; Olivo-Marin, J.-C. Tracking Algorithms Chase Down Pathogens. *Biotechnol. J.* **2009**, *4*, 838−45.
(38) Fox, E.; Sudderth, E. B.; Jordan, M. I.; Willsky, A. S. Bayesian Nonparametric Inference of Switching Dynamic Linear Models. *IEEE Trans. Signal Process.* **2011**, *59*, 1569−1585.
(39) Meister, G.; Fischer, U. Assisted RNP Assembly: SMN and PRMT5 Complexes Cooperate in the Formation of Spliceosomal UsnRNPs. *EMBO J.* **2002**, *21*, 5853−63.
(40) Holstege, F. C.; Jennings, E. G.; Wyrick, J. J.; Lee, T. I.; Hengartner, C. J.; Green, M. R.; Golub, T. R.; Lander, E. S.; Young, R. A. Dissecting the Regulatory Circuitry of a Eukaryotic Genome. *Cell* **1998**, *95*, 717−28.
(41) Zenklusen, D.; Larson, D. R.; Singer, R. H. Single-RNA Counting Reveals Alternative Modes of Gene Expression in Yeast. *Nat. Struct. Mol. Biol.* **2008**, *15*, 1263−71.
(42) Zhang, L.; Mykland, P.; Ait-Sahalia, Y. A Tale of Two Time Scales: Determining Integrated Volatility With Noisy High-Frequency Data. *J. Am. Stat. Assoc.* **2005**, *100*, 1394−1411.
(43) Hong, Y.; Li, H. Nonparametric Specification Testing for Continuous-Time Models with Applications to Term Structure of Interest Rates. *Rev. Financ. Stud.* **2005**, *18*, 37−84.
(44) Cho, J. S.; White, H. Generalized Runs Tests for the IID Hypothesis. *J. Econom.* **2011**, *162*, 326−344.
(45) Chen, B.; Hong, Y. Characteristic Function-Based Testing for Multifactor Continuous-Time Markov Models Via Nonparametric Regression. *Econom. Theory* **2010**, *26*, 1115−1179.
(46) Aït-Sahalia, Y.; Fan, J.; Jiang, J. Nonparametric Tests of the Markov Hypothesis In Continuous-Time Models. *Ann. Stat.* **2010**, *38*, 3129−3163.
(47) Remillard, B.; Papageorgiou, N. A.; Soustra, F. Copula-Based Semiparametric Models for Multivariate Time Series. *J. Multivariate Anal.* **2012**, *110*, 30−42.
(48) Calderon, C. P.; Arora, K. Extracting Kinetic and Stationary Distribution Information from Short MD Trajectories via a Collection of Surrogate Diffusion Models. *J. Chem. Theory Comput.* **2009**, *5*, 47.
(49) Calderon, C. P. On the Use of Local Diffusion for Path Ensemble Averaging in Potential of Mean Force Computations. *J. Chem. Phys.* **2007**, *126*, 084106.
(50) Calderon, C. P.; Janosi, L.; Kosztin, I. Using Stochastic Models Calibrated from Nanosecond Nonequilibrium Simulations to Approximate Mesoscale Information. *J. Chem. Phys.* **2009**, *130*, 144908.
(51) Calderon, C. P. Detection of Subtle Dynamical Changes Induced by Unresolved Conformational Coordinates in Single-Molecule Trajectories via Goodness-of-Fit Tests. *J. Phys. Chem. B* **2010**, *114*, 3242−3253.
(52) Hong, Y.; Li, H.; Zhao, F. Can the Random Walk Model be Beaten in Out-of-Sample Density Forecasts? Evidence from Intraday Foreign Exchange Rates. *J. Econom.* **2007**, *141*, 736−776.
(53) Calderon, C. P.; Martinez, J.; Carroll, R.; Sorensen, D. P-Splines Using Derivative Information. *Multiscale Model. Simul.* **2010**, *8*, 1562−1580.
(54) Claeskens, G.; Hjort, N. *Model Selection and Model Averaging*; Cambridge University Press: Cambridge, U.K., 2008.
(55) Kloeden, P.; Platen, E. *Numerical Solution of Stochastic Differential Equations*; Springer-Verlag: Berlin, 1992.
(56) Thompson, R. E.; Larson, D. R.; Webb, W. W. Precise Nanometer Localization Analysis for Individual Fluorescent Probes. *Biophys. J.* **2002**, *82*, 2775−83.
(57) Hamilton, J. *Time Series Analysis*; Princeton University Press: Princeton, NJ, 1994.
(58) Stengel, R. *Optimal Control and Estimation*; Dover Publications: Toronto, Ontario, Canada, 1994.
(59) Genovesio, A.; Liedl, T.; Emiliani, V.; Parak, W. J.; Coppey-Moisan, M.; Olivo-Marin, J.-C. Multiple Particle Tracking in 3-D+t Microscopy: Method and Application to the Tracking of Endocytosed

Quantum Dots. *IEEE Transactions on Image Processing* **2006**, *15*, 1062−70.
(60) Bertaux, N.; Marguet, D. Dynamic Multiple-Target Tracing to Probe Spatiotemporal Cartography of Cell Membranes. *Nat. Methods* **2008**, *5*, 687−694.
(61) Jaqaman, K.; Loerke, D.; Mettlen, M.; Kuwata, H.; Grinstein, S.; Schmid, S. L.; Danuser, G. Robust Single-Particle Tracking in Live-Cell Time-Lapse Sequences. *Nat. Methods* **2008**, *5*, 695−702.
(62) Sergé, A.; Bertaux, N.; Rigneault, H.; Marguet, D. Dynamic Multiple-Target Tracing to Probe Spatiotemporal Cartography of Cell Membranes. *Nature Methods* **2008**, *5*, 687−94.
(63) Jimenez, J.; Ozaki, T. An Approximate Innovation Method for the Estimation of Diffusion Processes from Discrete Data. *J. Time Series Analysis* **2006**, *27*, 77−97.
(64) Pavani, S. R.; Piestun, R. High-Efficiency Rotating Point Spread Functions. *Opt. Express* **2008**, *16*, 3484−3489.
(65) Adler, D.; Murdoch, D. RGL: 3D Visualization Device System (OpenGL). 2011; R package version 0.92.798.
(66) Saxton, M. J. Single-Particle Tracking: Connecting the Dots. *Nat. Methods* **2008**, *5*, 671−2.
(67) Calderon, C. P. Correcting for Bias of Molecular Confinement Parameters Induced by Small-Time-Series Sample Sizes in Single-Molecule Trajectories Containing Measurement Noise. *Phys. Rev. E* **2013**, *88*, 012707.
(68) Granger, C.; Joyeux, R. An Introduction to Long-Memory Time Series Models and Fractional Differencing. *J. Time Ser. Anal.* **1980**, *1*, 15−30.
(69) Lubelski, A.; Sokolov, I. M.; Klafter, J. Nonergodicity Mimics Inhomogeneity in Single Particle Tracking. *Phys. Rev. Lett.* **2008**, *100*, 250602.
(70) Liphardt, J.; Onoa, B.; Smith, S. B.; Tinoco, I.; Bustamante, C. Reversible Unfolding of Single RNA Molecules by Mechanical Force. *Science* **2001**, *292*, 733−7.
(71) Gerland, U.; Bundschuh, R.; Hwa, T. Mechanically Probing the Folding Pathway of Single RNA Molecules. *Biophys. J.* **2003**, *84*, 2831−40.
(72) Wen, J.-D.; Lancaster, L.; Hodges, C.; Zeri, A.-C.; Yoshimura, S. H.; Noller, H. F.; Bustamante, C.; Tinoco, I. Following Translation by Single Ribosomes One Codon at a Time. *Nature* **2008**, *452*, 598−603.
(73) Qu, X.; Wen, J.-D.; Lancaster, L.; Noller, H. F.; Bustamante, C.; Tinoco, I. The Ribosome Uses Two Active Mechanisms to Unwind Messenger RNA During Translation. *Nature* **2011**, *475*, 118−21.
(74) Zhang, W.; Dunkle, J.; Cate, J. Structures of the Ribosome in Intermediate States of Ratcheting. *Science* **2009**, *325*, 1014.
(75) Ben-Shem, A.; Jenner, L.; Yusupova, G.; Yusupov, M. Crystal Structure of the Eukaryotic Ribosome. *Science* **2010**, *330*, 1203−9.
(76) Müller, M. J. I.; Klumpp, S.; Lipowsky, R. Tug-of-War as a Cooperative Mechanism for Bidirectional Cargo Transport by Molecular Motors. *Proc. Natl. Acad. Sci. U.S.A.* **2008**, *105*, 4609−14.
(77) Welte, M. A. Bidirectional Transport: Matchmaking for Motors. *Curr. Biol.* **2010**, *20*, R410−3.